**Supporting Information**

# Room-temperature reversible F-ion batteries based on sulfone electrolyte with mild anion acceptor additive

**Yifan Yu [1,2,3], Meng Lei [1,3], Chilin Li [1,2,3,*]**

[1] State Key Laboratory of High Performance Ceramics and Superfine Microstructure, Shanghai Institute of Ceramics, Chinese Academy of Sciences, 585 He Shuo Road, Shanghai 201899, China. Email: chilinli@mail.sic.ac.cn

[2] Center of Materials Science and Optoelectronics Engineering, University of Chinese Academy of Sciences, Beijing 100049, China.

[3] CAS Key Laboratory of Materials for Energy Conversion, Shanghai Institute of Ceramics, Chinese Academy of Sciences, Shanghai 201899, China.

## Experiments

### Materials preparation

**Materials.** All compounds including solvents were acquired from Aladdin, Sigma-Aldrich, Adamas, Sinopharm Chemical Reagent Co., Ltd and MTI Corporation and they were used as received. The electrode materials contain $CuF_2$ (Adamas, 98%), Pb foil (0.3 mm thick, ≧99.999%), Ketjen Black (KB-C, MTI Corporation), poly(vinyl difluoride) (PVDF, Sigma-Aldrich), and Super P (SP, MTI Corporation).

**Preparation of electrolyte.** Firstly, 0.5 M 6-Thioguanine (abbreviated as TG, Aladdin, 98%) was dissolved in dimethyl sulfoxide (DMSO, Aladdin, 99.9%) under vigorously magnetic stirring for 6 h to get a homogeneous TG/DMSO solution. Then 0, 0.5 M, 1.0 M, 1.5 M or 2.0 M CsF (Aladdin, 99.9%) was added into the solution and the white electrolytes were obtained after stirring overnight. According to their chemical compositions, these electrolytes were abbreviated as CTD0, CTD1, CTD2, CTD3 and CTD4, respectively. We also tried the ether solvents (e.g. G4), but TG was seemingly insoluble in ether.

**Preparation of $CuF_2$ composite cathode.** Commercial anhydrous $CuF_2$ and KB-C

were taken to acquire the $CuF_2$ composite cathode (noted as $CuF_2$-c) with a mass ratio of 8:2 via high energy ball milling with a rate of 600 rpm for 5 h.

**Electrochemical measurement**

$CuF_2$-c was mixed with SP and PVDF, which serve as conductive carbon and binder respectively, under a mass ratio of 7:2:1. PVDF was dissolved in 1-methyl-2-pyrrolidinone (NMP, Sinopharm Chemical Reagent Co., Ltd, ≧99.0%) under a mass concentration of 1 mg/20 μL in advance before the mixing process. Then the mixture was bladed on the pure Al foil and dried in vacuum at 60 ℃ for overnight. Glassfibre from Whatman was used as the separator. The CR2032-type coin cells were assembled in a glove box filled with Ar ($O_2$, $H_2O$ < 0.1 ppm, Vigor). The electrochemical window of electrolytes was measured by linear sweep voltammetry on an electrochemical workstation (Princeton Versa STAT3). The ionic conductivity of electrolytes was gauged through an ionic conductivity meter (DDSJ-308A) at room temperature. Galvanostatic charge-discharge cycling performance was carried out with a discharge cut-off voltage of -0.15 V (vs. $Pb^{2+}$/Pb) and a charge cut-off capacity of 150 mA h $g^{-1}$ at room temperature at a current density of 50 mA/g on the Land multichannel battery testing system (CT2001A). The symmetric cells by taking the mixture of Sn and $SnF_2$ (with a mass ratio of 1:1) as electrodes were employed to determine the $F^-$ transport number ($t_F$) on VersaSTAT3 workstation s with a DC polarization voltage of 10 mV. The $t_F$ value could be obtained according to the following equation:

$$t_F = \frac{I_{SS}(\Delta V - I_0 R_0)}{I_0(\Delta V - I_{SS} R_{ss})}$$

where ΔV is 10 mV, $I_0$ and $I_{ss}$ are the current responses at the initial and steady states, $R_0$ and $R_{ss}$ are the corresponding resistances at the initial and steady states.

**Materials characterization**

**Electrolyte characterization.** To provide an insight into the interaction mechanism of TG with CsF, the TG, CsF and electrolyte CTD were used for nuclear magnetic resonance (NMR) spectroscopy measurement. The $^1H$, $^{13}C$, and $^{19}F$ spectra were

acquired from a Bruker Avance III HD 400 MHz spectrometer with deuterated reagents of $CD_3CN$, DMSO-d6 and $CDCl_3$ respectively. Fourier transform infrared (FTIR) spectroscopy was collected by Nicolet iS10 in a wavenumber range from 4000 to 400 $cm^{-1}$.

**Electrode characterization.** The phase evolution of Pb anodes before and after cycling was analyzed by X-ray diffractometer (XRD, Bruker, D8 Discover) in a scanning 2θ range of 10-80 ° at a rate of 10°/min with Cu K$\alpha$ radiation. The chemical composition and elemental valence of the pristine and cycled $CuF_2$-c composites were detected by X-ray photoelectron spectroscopy (XPS, ESCAlab-250) with an Al anode source. Further information of the microstructure and spatial distribution of phases for cathodes were disclosed by high-resolution transmission electron microscopy (HRTEM) images and selected area electron diffraction (SAED) patterns collected from JEOL JSM-6700F, operated with an acceleration voltage of 200 kV. All the *ex-situ* characterizations of the cycled electrode samples were prepared by disassembling the cycled cells in the Ar-filled glove box and then repeatedly washed with DMSO to remove the residual salts. These samples were transferred to the testing chamber after drying and sealing.

**Theoretical calculation**

DFT calculations were implemented by adopting the Vienna Ab initio Simulation Package (VASP). Projector augmented wave pseudo-potentials were used to describe the interaction between valence electrons and ions. Additionally, the exchange-correlation interaction was treated by Perdew-Burke-Ernzerhof (PBE) of the generalized gradient approximation (GGA) function. The cutoff energy was set as 500 eV and the structures were relaxed until the energy variation is less than $10^{-6}$ eV. The force convergence criterion was set as 0.02 eV/Å. The adsorption energy ($E_a$) for TG to F was described as $E_a = E_{TG+F} - (E_{TG} + E_F)$, where $E_{TG+F}$ is the total energy of adsorption system after geometry optimization, $E_{TG}$ and $E_F$ are the energies of TG molecule and F atom respectively. The van der Waal (vdw) interaction was described via the DFT-D3 correction method of Grimme.

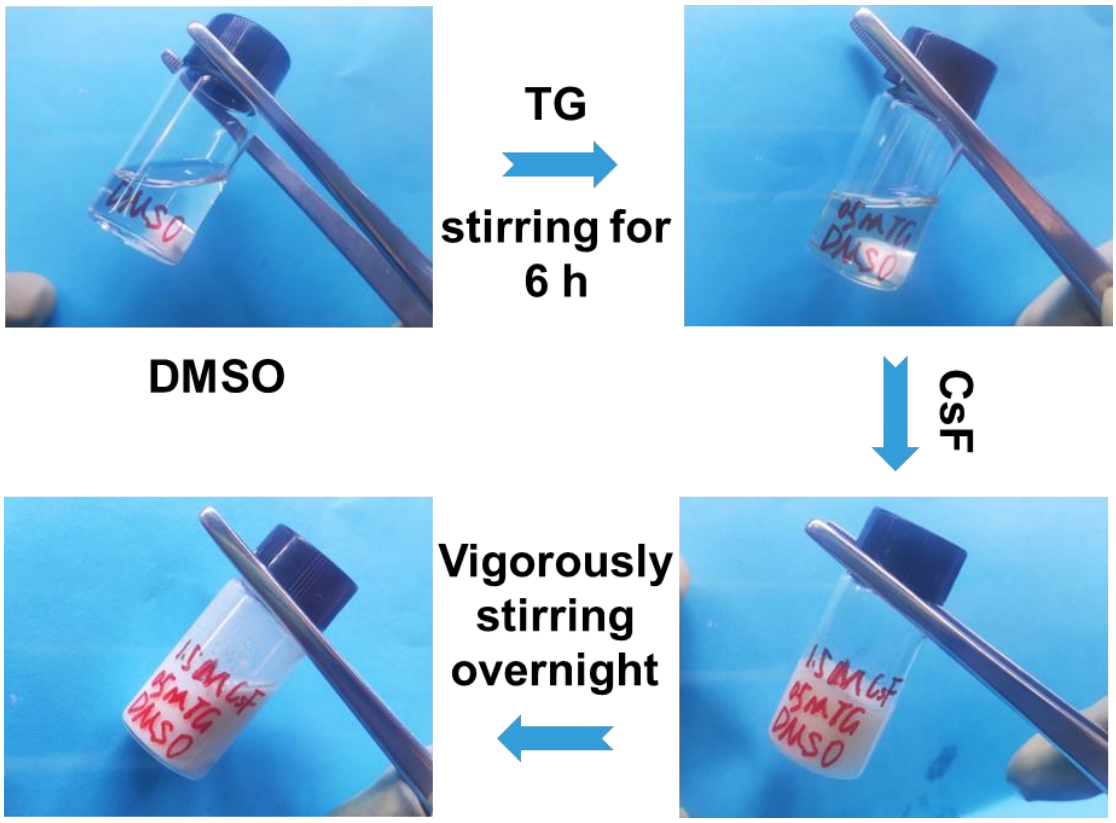


**Figure S1**. Optical photos of the preparation process of electrolyte.

a

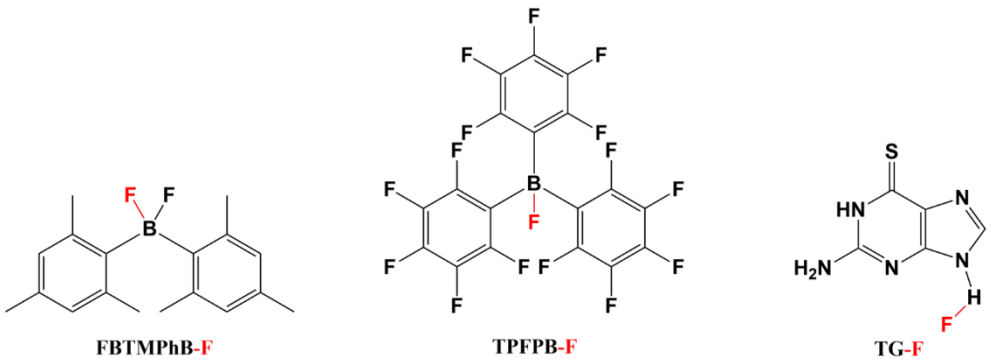


b

| AA-F | Adsorption energy (kJ/mol) | Reference |
|---|---|---|
| FBTMPhB-F | -312.3 | J. Electrochem. Soc., 164 (14) A3702-A3708 (2017) |
| TPFPB-F | -406.0 | J. Electrochem. Soc., 164 (14) A3702-A3708 (2017) |
| TG-F | -133.0 | This work |

**Figure S2**. (a) Illustration of adsorption situations of different AAs to F. (b) Corresponding adsorption energies of AA-F complexes. The data of FBTMPhB-F and TPFPB-F both refer to the work reported by Konishi et al..[1]

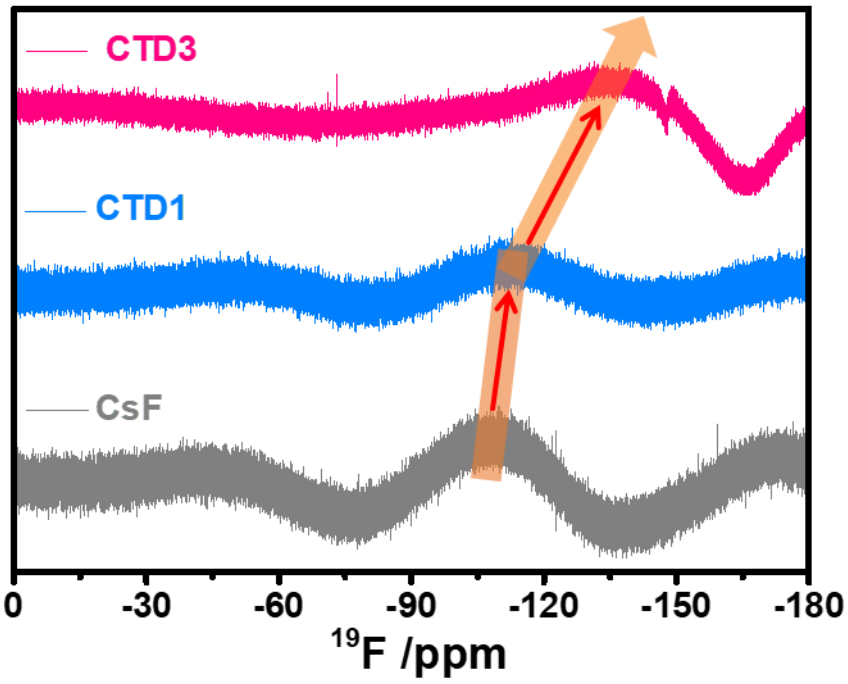


**Figure S3**. $^{19}F$ NMR spectra of CsF, CTD1 and CTD3. The chemical shift values for CsF, CTD1 and CTD3 are -108 ppm, -113 ppm and -137 ppm respectively.

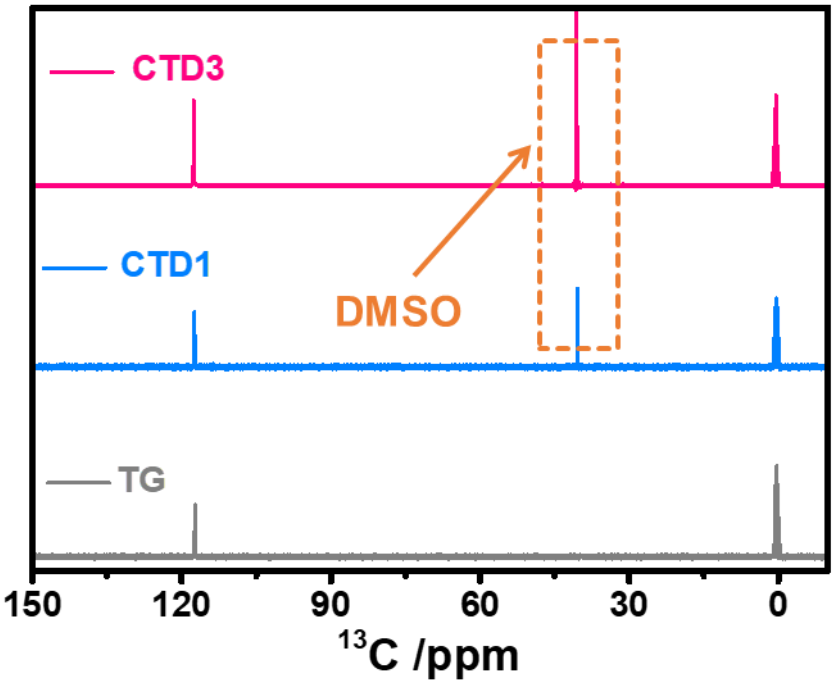


**Figure S4**. $^{13}C$ NMR spectra of TG, CTD1 and CTD3. There is no peak shift for CTD1 and CTD3 and the newly added peak at 40.5 ppm is the signal of C from DMSO.

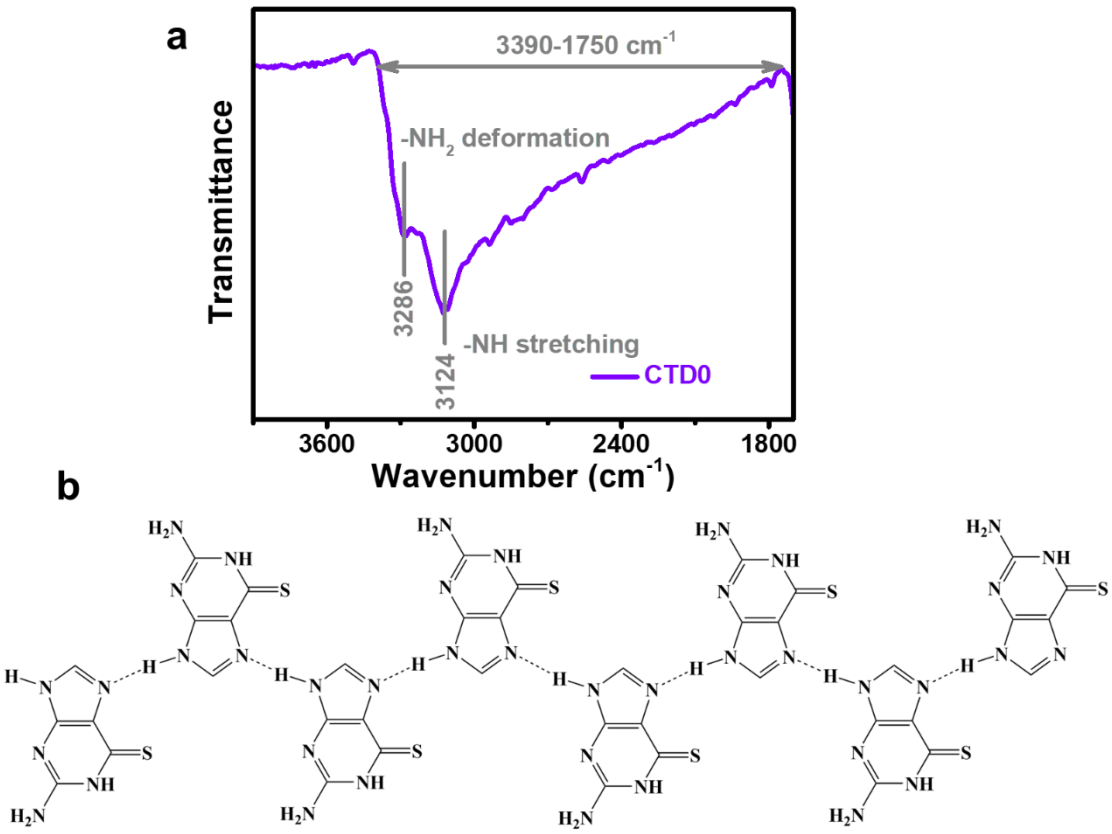


**Figure S5**. (a) FTIR curve of CTD0. A broad band in the region from 3390 to 1750 $cm^{-1}$ is observed, and it indicates the formation of TG complex. This complex is formed via the hydrogen bonds between TG molecules. (b) Scheme of the hydrogen-bonded TG chains in CTD0.

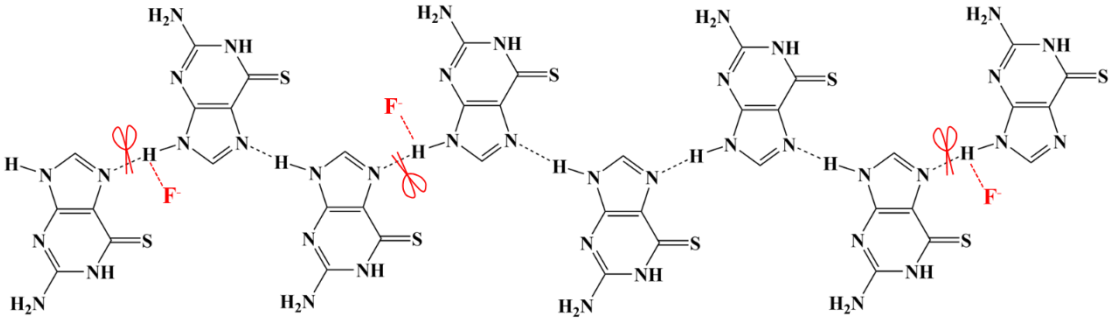

**Figure S6**. Scheme of the cutting of hydrogen bonds in TG chains in CTD3.

| Ionic conductivity of electrolyte based on AA strategy | | |
|---|---|---|
| **Electrolyte** | **Ionic conductivity (mS/cm, RT)** | **Ref.** |
| 0.15 M CsF+ 0.5 M TPhBX Sx | 0.046 | 2 |
| Sat-CsF +0.5 M DiOB-An G4 | 0.0032 | 3 |
| Sat-CsF +0.5 M DiOB-Py G4 | 0.027 | 3 |
| CTD1 | 2.11 | This work |
| CTD2 | 2.40 | This work |
| CTD3 | 1.75 | This work |
| CTD4 | 1.54 | This work |

**Figure S7**. Ionic conductivities of F-ion electrolytes based on AA strategy at room temperature reported by literatures,[2,3] and the sulfone electrolytes designed in this work.

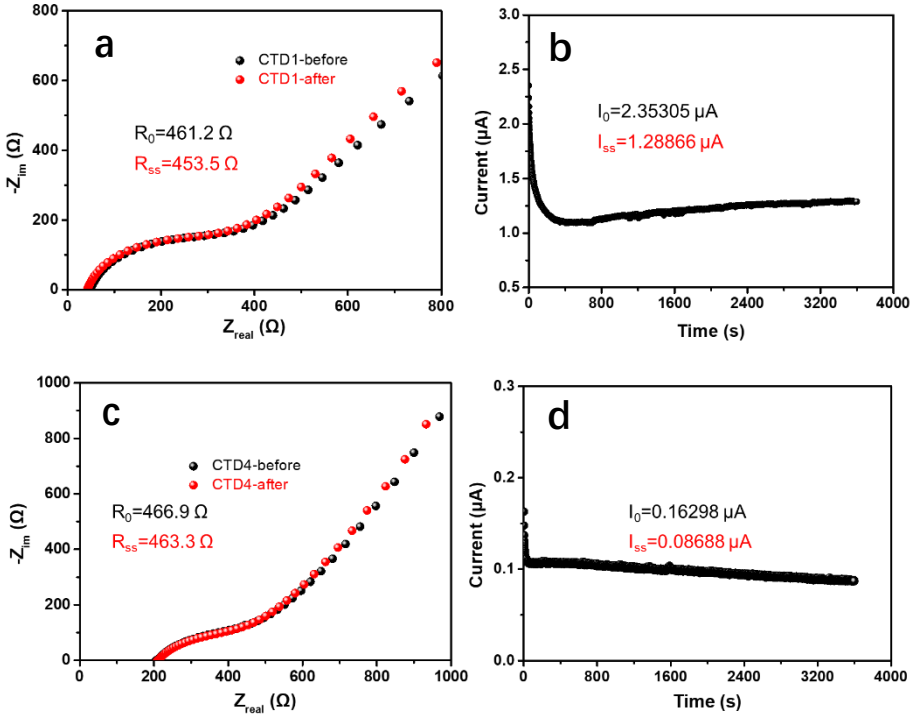

**Figure S8.** Impedance spectra for (a) CTD1 and (c) CTD 4 before and after polarization measurement. DC polarization measurement and current response with time for (b) CTD1 and (d) CTD 4.

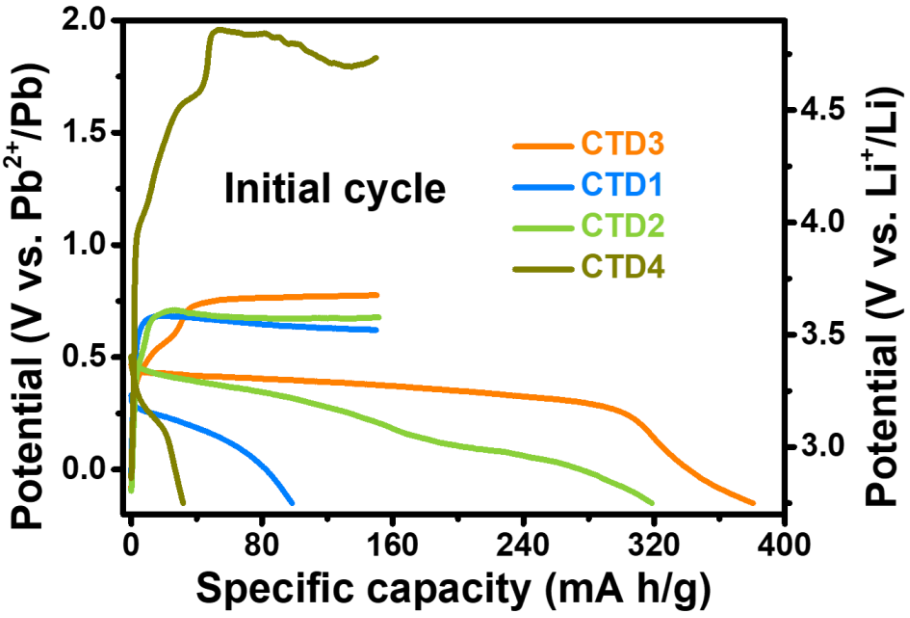


**Figure S9**. Charge/discharge curves of $CuF_2$|CTDn|Pb cells during the initial cycle.

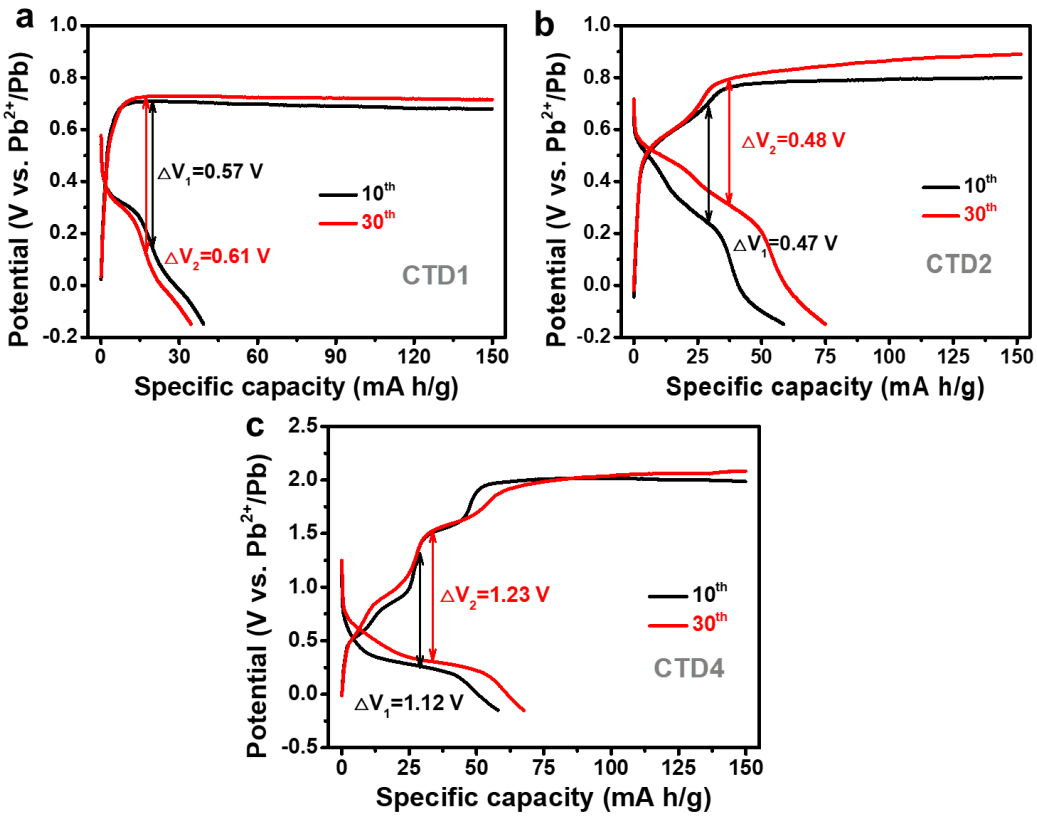


**Figure S10**. Electrochemical curves of (a) $CuF_2$|CTD1|Pb, (b) $CuF_2$|CTD2|Pb, (c) $CuF_2$|CTD4|Pb cells during the $10^{th}$ and $30^{th}$ cycles.

| Initial capacity (mA h/g) | Current density | Cycle number | Operating temperature (°C) | $10^{th}$ discharge capacity (mA h/g) | Ref. |
|---|---|---|---|---|---|
| 316 | 7.55 mA/g | 30 | 25 | 139.3 | 4 |
| 75 | 10 mA/g | 100 | 25 | 55.5 | 5 |
| 218 | 30.2 mA/g | 10 | 55 | 30 | 2 |
| 500 | 26.4 mA/g | 10 | 25 | 260 | 6 |
| 427 | 7.55 mA/g | 10 | 25 | 132 | 7 |
| 60 | 0.01 mA/cm$^2$ | 7 | 25 | 33.3 | 8 |
| 189 | 0.01 mA | - | 25 | - | 9 |
| 375 | 0.01 mA | - | 25 | - | 10 |
| 319 | 7.55 mA/g | 3 | 25 | 98 | 11 |
| 40 | 15.1 mA/g | 7 | 25 | 75 | 12 |
| 322 | 7.55 mA/g | 3 | 25 | 53 | 13 |
| 280 | 7.55 mA/g | 8 | 25 | 95 | 14 |
| **380.5** | **50 mA/g** | **40** | **25** | **126.8** | **This work** |

**Figure S11**. Performance comparison between reported FIBs based on liquid electrolytes and our FIB.[2, 4-14]

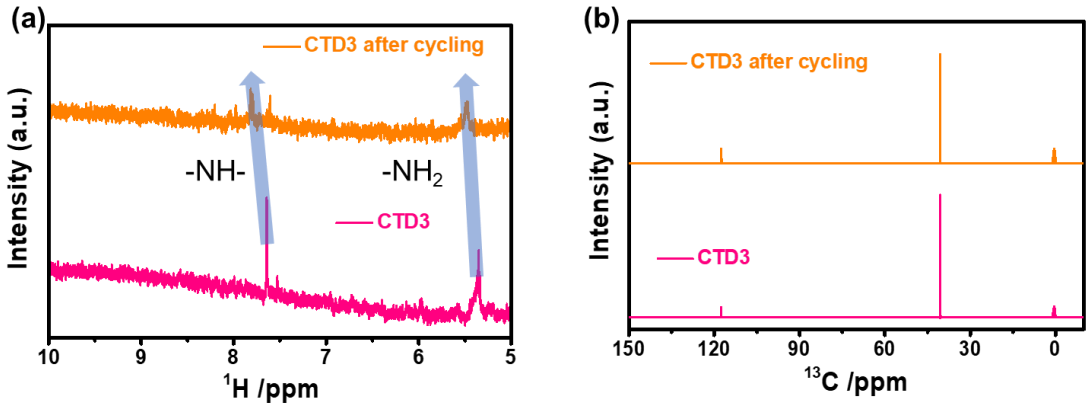


**Figure S12.** (a) $^{1}$H and (b) $^{13}$C NMR spectra of as-prepared CTD3 and cycled CTD3 after 10 cycles

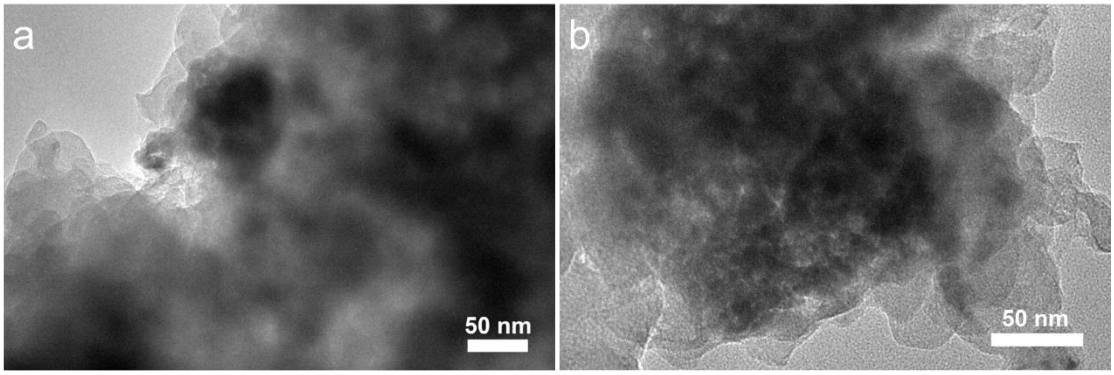


**Figure S13**. TEM images of cathode morphology in different areas after discharging.

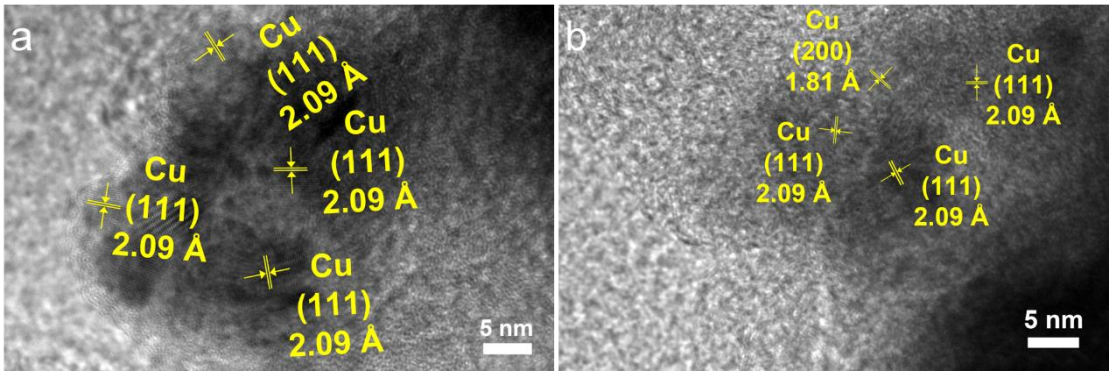


**Figure S14**. HRTEM images of discharged cathode in different areas.

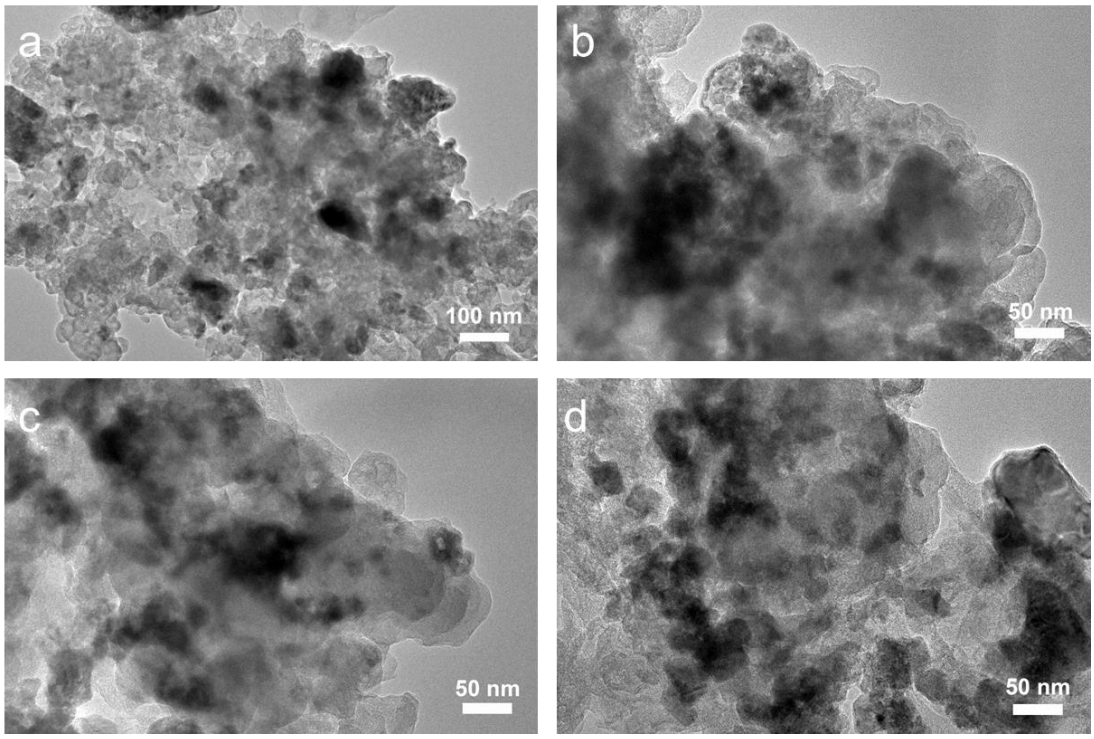


**Figure S15**. TEM images of charged cathode in different areas at different scales of (a) 100 nm and (b-d) of 50 nm.

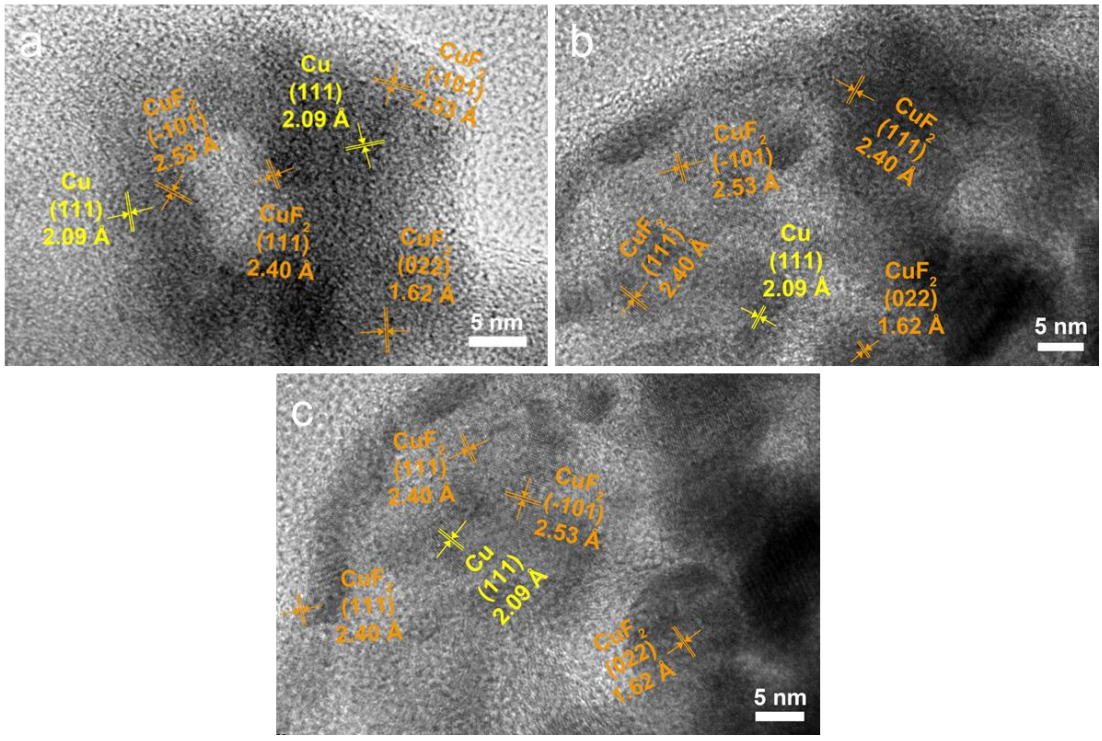


**Figure S16**. HRTEM images of charged cathode in different areas.

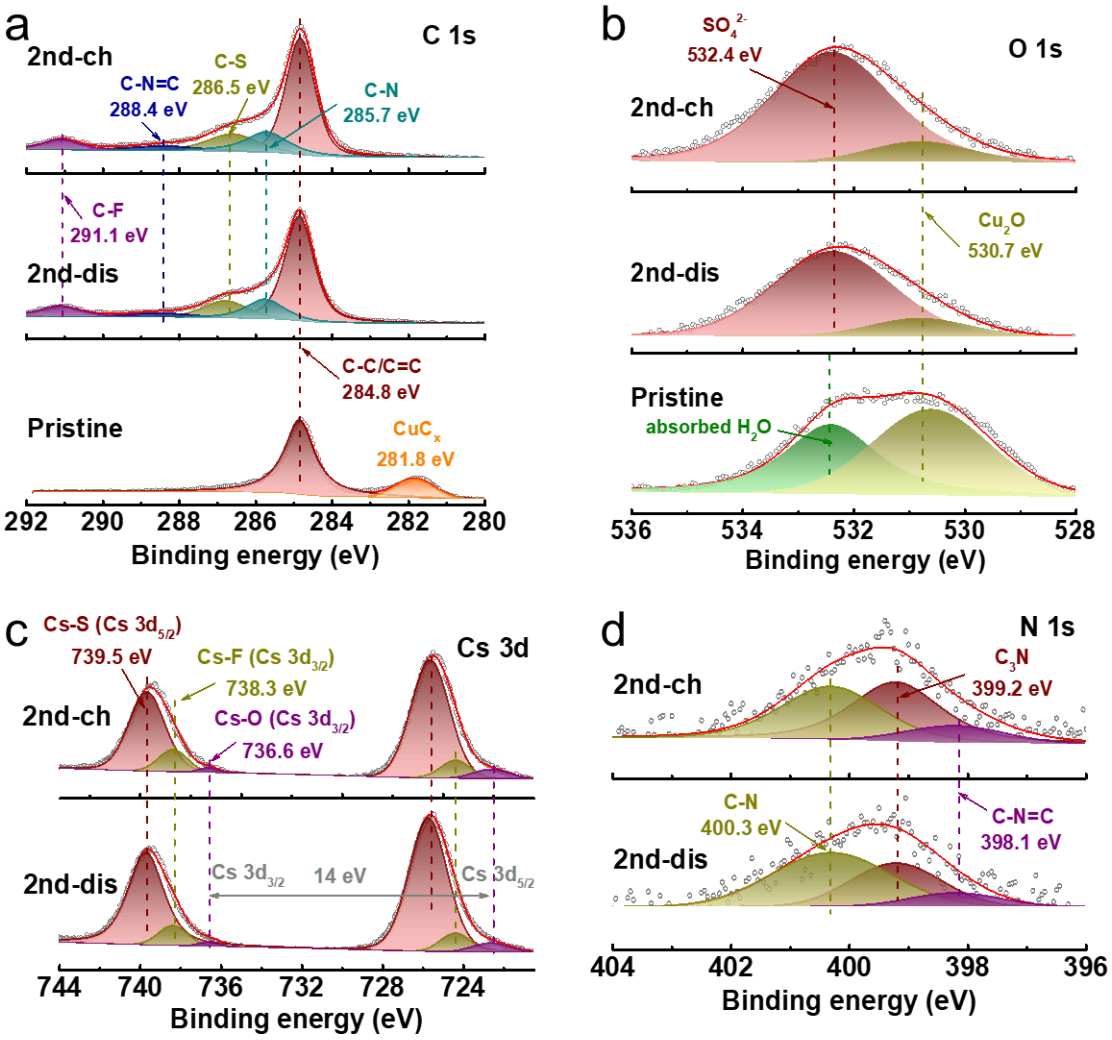


**Figure S17**. XPS spectra of pristine $CuF_2$ cathode and cycled cathodes when CTD1 serves as the electrolyte: (a) C 1s, (b) O 1s, (c) Cs 3d and (d) N 1s.

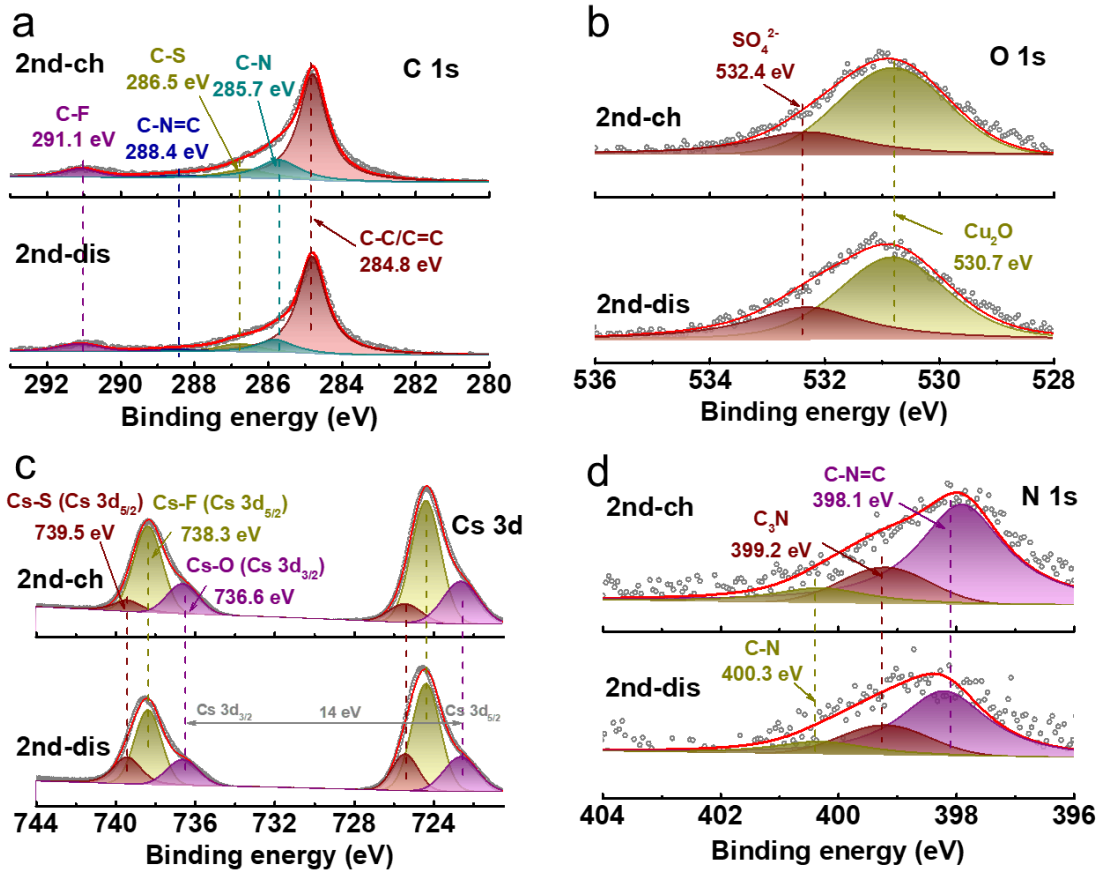


**Figure S18**. XPS spectra of cycled $CuF_2$ cathodes when CTD3 serves as the electrolyte: (a) C 1s, (b) O 1s, (c) Cs 3d and (d) N 1s.

## References


[1] H. Konishi, T. Minato, T. Abe, Z. Ogumi, *J. Electrochem. Soc.* **2017,** *164*, A3702-A3708.

[2] A. Celik Kucuk, T. Yamanaka, T. Abe, *J. Mater. Chem. A* **2020,** *8*, 22134-22142.

[3] A. Celik Kucuk, T. Abe, *J. Fluorine Chem.* **2020,** *240*, 109672.

[4] A. Celik Kucuk, T. Yamanaka, Y. Yokoyama, T. Abe, *J. Electrochem. Soc.* **2021,** *168*, 010501.

[5] S. Zhang, T. Wang, J. Zhang, Y. Miao, Q. Yin, Z. Wu, Y. Wu, Q. Yuan, J. Han, *ACS Appl. Mater. Interfaces* **2022,** *14*, 24518-24525.

[6] T. Yamamoto, K. Matsumoto, R. Hagiwara, T. Nohira, *ACS Appl. Energy Mater.* **2019,** *2*, 6153-6157.

[7] H. Konishi, A. C. Kucuk, T. Minato, T. Abe, Z. Ogumi, *J. Electroanal. Chem.* **2019,** *839*, 173-176.

[8] V. K. Davis, C. M. Bates, K. Omichi, B. M. Savoie, N. Momčilović, Q. Xu, W. J. Wolf, M. A. Webb, K. J. Billings, N. H. Chou, S. Alayoglu, R. K. McKenney, I. M. Darolles, N. G. Nair, A. Hightower, D. Rosenberg, M. Ahmed, C. J. Brooks, T. F. Miller, R. H. Grubbs, S. C. Jones, *Science* **2018,** *362*, 1144-1148.

[9] F. Gschwind, Z. Zao-Karger, M. Fichtner, *J. Mater. Chem. A* **2014,** *2*, 1214-1218.

[10] F. Gschwind, J. Bastien, *J. Mater. Chem. A* **2015,** *3*, 5628-5634.

[11] H. Konishi, T. Minato, T. Abe, Z. Ogumi, *J. Phys. Chem. C* **2019,** *123*, 10246-10252.

[12] J. L. Andrews, E. T. McClure, K. K. Jew, M. B. Preefer, A. Irshad, M. J. Lertola, D. D. Robertson, C. Z. Salamat, M. J. Brady, L. F. J. Piper, S. H. Tolbert, J. Nelson Weker, B. F. Chmelka, B. S. Dunn, S. R. Narayan, W. C. West, B. C. Melot, *ACS Energy Lett.* **2022,** *7*, 2340-2348.

[13] H. Konishi, T. Minato, T. Abe, Z. Ogumi, *ChemistrySelect* **2020,** *5*, 4943-4946.

[14] A. Celik Kucuk, T. Yamanaka, T. Abe, *Solid State Ionics* **2020,** *357*, 115499.